Along-strike structure of the Costa Rican convergent margin from seismic a refraction/reflection survey: Evidence for underplating beneath the inner forearc

J. St. Clair[1], W. S. Holbrook[1], H. J. A. Van Avendonk[2], and D. Lizarralde[3]

[1]Department of Geology and Geophysics, University of Wyoming, Laramie, WY, USA, [2]Jackson School of Geosciences, University of Texas Institute for Geophysics, Austin, Texas, USA, [3]Department of Geology and Geophysics, Woods Hole Oceanographic Institution, Woods Hole, Massachusetts, USA

Abstract The convergent margin offshore Costa Rica shows evidence of subsidence due to subduction erosion along the outer forearc and relatively high rates of uplift ($\sim$3–6 mm/yr) along the coast. Recently erupted arc lavas exhibit a low ^{10}Be signal, suggesting that although nearly the entire package of incoming sediments enters the subduction zone, very little of that material is carried directly with the downgoing Cocos plate to the magma generating depths of the mantle wedge. One mechanism that would explain both the low ^{10}Be and the coastal uplift is the underplating of sediments, tectonically eroded material, and seamounts beneath the inner forearc. We present results of a 320 km long, trench-parallel seismic reflection and refraction study of the Costa Rican forearc. The primary observations are (1) margin perpendicular faulting of the basement, (2) thickening of the Cocos plate to the northwest, and (3) two weak bands of reflections in the multichannel seismic (MCS) reflection image with travel times similar to the top of the subducting Cocos plate. The modeled depths to these reflections are consistent with an $\sim$40 km long, 1–3 km thick region of underplated material $\sim$15 km beneath some of the highest observed coastal uplift rates in Costa Rica.

1. Introduction

A primary goal in convergent margin research is to understand the mass balance of crustal material at subduction zones [*von Huene and Scholl*, 1991] where oceanic crust, along with pelagic and terrigenous sediments and a significant amount of continental material from the overriding plate, is recycled into the mantle [*Scholl and von Huene*, 2007]. The release of fluids and volatiles from the subducting material in the mantle wedge facilitates arc magmatic processes [*Schmidt and Poli*, 1998], resulting in the addition of new crustal material to the overriding plate. A better quantitative estimate of the crustal material flux into the mantle in subduction zones will help our understanding of the global mass balance and the chemical evolution of the Earth [*Albarède*, 1998].

Two types of convergent margins have been recognized: (1) The erosive margin, which exhibits a net loss of mass through time, and (2) the accretionary margin, which gains mass through time. Erosive margins are recognized on the basis of landward trench migration and forearc subsidence while accretionary margins are recognized by seaward migration of the trench and large accretionary wedges [*Clift and Vannucchi*, 2004]. Many convergent margins may experience simultaneous outer-forearc erosion and subsidence as well as inner fore-arc uplift associated with mass underplating [*Clift and Hartley*, 2007; *Collot et al.*, 2008; *Sak et al.*, 2009].

The convergent margin of Costa Rica is considered to be erosive on the basis of the subsidence recorded by upper slope sediments observed near the trench during ODP leg 170 [*Vannucchi et al.*, 2001, 2003] and trench parallel extensional faults observed in outer-forearc seismic images [*Meschede et al.*, 1999]. Conversely, onshore studies of marine terraces document significant rates of Quaternary uplift [*Fisher et al.*, 1998; *Sak et al.*, 2009]. These studies have attributed coastal uplift to the subduction of topographic highs on the Cocos plate. An alternative explanation is the underplating of sediments, seamounts, and tectonically eroded material beneath actively uplifting regions of the forearc, a process that may also explain why the

[10]Be signature in Costa Rica arc magmas is quite low [*Morris et al.*, 1990] even though the shallow sediments from the Cocos plate that contain the cosmogenic [10]Be underthrust the prism [e.g., *Vannucchi et al.*, 2001].

In this study, we present new observations from the "Osa" line, an along-strike, coincident seismic reflection and refraction survey of the forearc region offshore Costa Rica (Figure 1). We image along strike variations in Moho depth, margin wedge thickness, and reflectivity along the interface between the overriding Caribbean plate and the subducting Cocos plate. We present two alternative velocity models consistent with the refraction data and use these to determine depths to a reflective zone observed near the plate interface in the reflection image. We interpret this reflective zone to evidence for spatially variable underplating of subducted material at ∼15 km depth.

2. Tectonic Setting

The Middle American Trench (MAT) is formed where the Cocos plate subducts beneath the Caribbean plate at ∼8.5 cm/yr to the NNE [*DeMets*, 2001]. The Cocos plate displays along-strike trends in age, origin, and bathymetry that are correlated with trends observed in the overriding Caribbean plate [*von Huene et al.*, 2000].

2.1. Cocos Plate

Offshore Costa Rica, the Cocos plate is comprised of three distinct tectonic provinces whose boundaries are evident from magnetic anomalies [*Barckhausen et al.*, 2001]. The oceanic crust offshore northwest Nicoya Peninsula formed at the East Pacific Rise (EPR) and is 24 Ma where it enters the MAT; spreading fabric here is parallel to the trench and the seafloor morphology, characteristic of fast-spreading crust, is smooth. A transition from EPR crust to the oldest crust formed at the Cocos-Nazca spreading center (CNS-1) is marked by a small fracture zone trace (Figure 1), possibly a remnant of the 23 Ma Farallon plate breakup. Here the spreading fabric is perpendicular to the trench and the age of the crust at the trench decreases from 22.5 to 20.5 Ma. Around 19.5 Ma, the CNS shifted to a more N-S spreading direction recorded in a ridge jump that separates CNS-1 from the younger CNS-2 crust (Figure 1). Here, the spreading fabric is oblique to the trench and the age decreases from 19 Ma at the ridge jump to 15 Ma offshore Osa peninsula [*Barckhausen et al.*, 2001].

The three morphologic segments that have been identified outboard the MAT on the basis of seafloor bathymetry correspond to a similar segmentation observed in the overriding Caribbean plate [*von Huene et al*, 2000]. The "smooth" segment, mostly void of seamounts, begins in the EPR derived crust and terminates at the Fisher ridge. Previous seismic studies indicate that the EPR derived crust is ∼6km thick [*Van Avendonk et al.*, 2011; *Ivandic et al.*, 2010]. Opposite this segment, the continental shelf shows a similarly smooth topography. Between the Fisher ridge and the Cocos ridge, the "seamount" segment is characterized for 40% seamount coverage of Galapagos affinity [*Werner et al.*, 1999]. Landward of this segment, "furrows" or "scallops" aligned in the direction of convergence with the major seamount chains record the subduction of seamounts [*von Huene et al.*, 2000]. The southernmost segment is dominated by Cocos Ridge, an ∼21 km thick [*Walther*, 2003] aseismic ridge interpreted to be the trace of the Galapagos hotspot [*Werner et al.*, 2003]. Landward of the trench, subduction of the Cocos Ridge causes a broad domal uplift in the upper plate near the Osa peninsula [*LaFemina et al.*, 2009].

2.2. Caribbean Plate

The Caribbean plate at Costa Rica is predominantly composed of the 88–90 Ma oceanic plateau known as the Caribbean Large Igneous Province (CLIP) [*Guinta and Beccaluva*, 2006; *Buchs et al.*, 2010]. Onshore basement exposures in Costa Rica are generally confined to the western margin where igneous rocks of similar composition to the CLIP are found [*Alvarado et al.*, 1997; *Sinton et al.*, 1997; *Denyer and Gazel*, 2009; *Buchs et al.*, 2010]. The most studied of these exposures is the Nicoya Complex, an oceanic terrain similar in age to the CLIP [*Sinton et al.*, 1997], which is observed in several locations along the Nicoya Peninsula. Offshore seismic refraction surveys of the forearc show either a one or two-layer margin wedge overlain by a layer of 1.8–2.9 km/s sediments of variable thickness [*Ye et al.*, 1996; *Christeson et al.*, 1999; *Zhu et al.*, 2009]. Velocities in the upper margin wedge have been observed to increase landward and range from ∼4 to 6 km/s while velocities up to 6.6 km/s have been observed in the lower margin wedge. The seismically observed
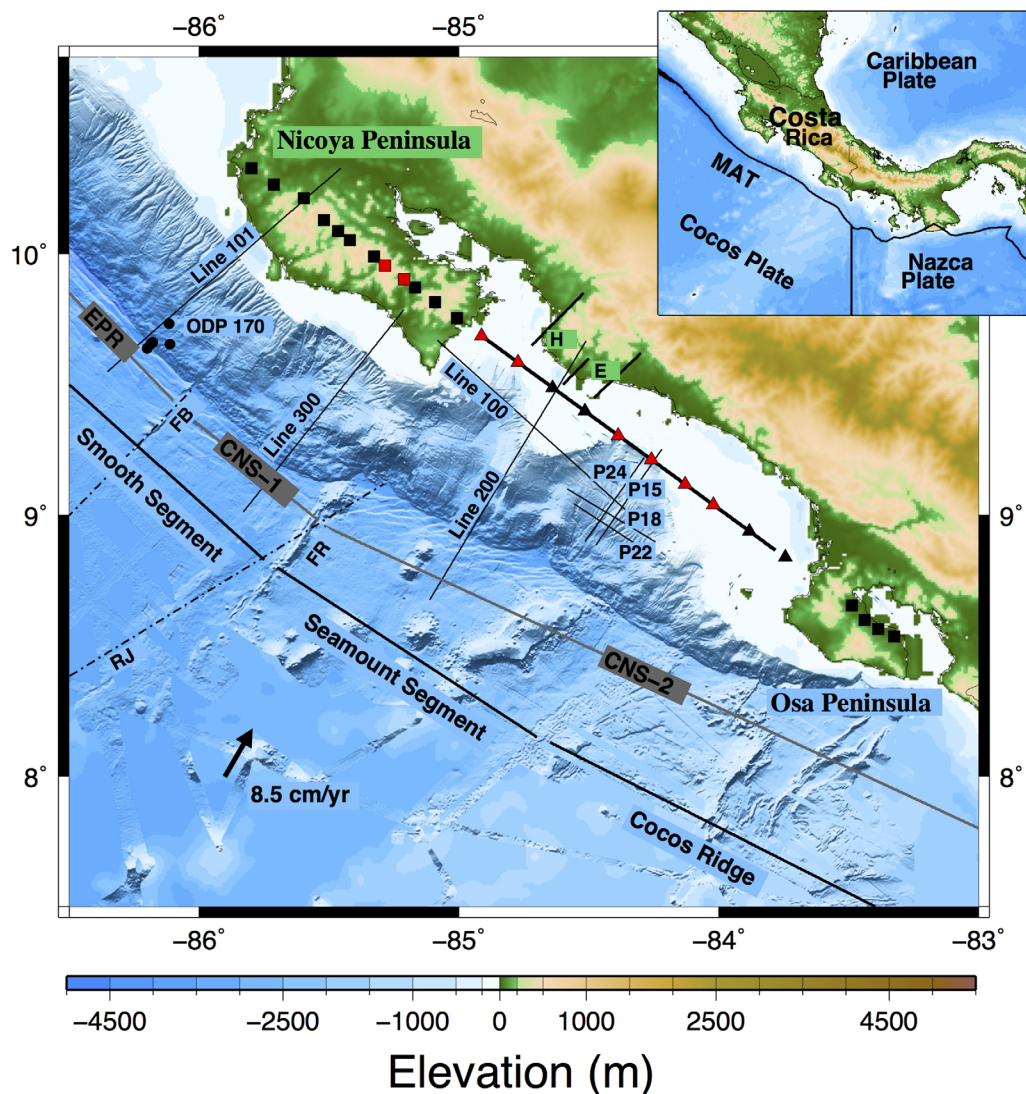
Figure 1. Map showing the MAT at Costa Rica and the location of the "Osa" line. Reftek and OBS locations are shown as squares and triangles, red symbols indicate instruments discussed in the text and shown in Figure 7. Thick black line running between Nicoya and Osa peninsulas shows the extent of shooting. Morphologic segmentation is shown with black lines after *von Huene et al.*, [2000]. Dashed lines show Cocos plate boundaries. RJ = ridge jump separating CNS-1 and CNS-2 derived crust, FB = Farallon plate break up separating CNS-1 and EPR crust after *Barckhausen et al.* [2001]. H = Herradura block, E= Esterillos block after *Sak et al.* [2009]. Calculated uplift rates for the Esterillos block are ~3.1–4.0 mm/yr [*Sak et al.*, 2009]. Thin black lines show approximate locations of previous surveys discussed in text; Line 101 after *Christeson et al.* [1999]; Lines 100, 200, and 300 after *Ye et al.* [1996]; P15, P18, P22, and P24 after *Zhu et al.* [2009]. Location of ODP leg 170 holes are shown as black dots. Regional setting of the MAT is shown in the inset.

margin wedge extends out to the trench and has been interpreted to be the offshore extension of the Nicoya Complex [e.g., *Hinz et al.*, 1996; *Christeson et al.*, 1999].

2.3. Subducting Sediments

Offshore Costa Rica the Cocos plate is overlain by 400–600 m of carbonates and hemipelagic sediments [*Patino et al.*, 2000; *Van Avendonk et al.*, 2011; *Walther*, 2003]. During ODP leg 170, the subduction fault along with nearly the complete package of sediments was penetrated beneath the margin wedge at site 1043 (Figure 1) and demonstrated the almost complete subduction of incoming sediments ant the MAT. Additionally, several seismic reflection images along the MAT have imaged packages of sediments along the décollement at distances up to 50 km inboard of the trench [e.g., *Zhu et al.*, 2009]. The observation that mass is not being accumulated at the trench, combined with the widespread subsidence related "scallops" or "furrows" along the lower to middle continental slope [*Ranero and von Huene*, 2000; *von Huene et al.*, 2000],

strongly suggest that erosion rather than accretion has been the dominant process effecting the MAT at Costa Rica since at least the Miocene [*Meschede et al.*, 1999].

The results of ODP leg 170 also present a significant mystery related to the final fate of the subducting sediment column. Site 1043 penetrated a nearly complete package of subducted sediments beneath the forearc basement demonstrating that the vast majority of sediments reaching the MAT are entering the subduction fault [*Vannucchi et al.*, 2001]. At site 1042, shallow water sediments overlain by deep water depositions demonstrate a history of subsidence along the outer forearc indicating a net loss of mass [*Vannucchi et al.*, 2001]. The fate of subducting sediments, and presumably tectonically eroded material from the outer forearc, is not yet clear. [10]Be concentrations in the incoming sediments are high and yet the concentrations in the recently erupted lavas along the arc are low [*Morris et al.*, 2002; *Carr et al.*, 2007]. [10]Be has a half-life of 1.5 Myr [*Morris et al.*, 1990]; given that the trench is roughly 200 km updip from the active volcanic arc and the convergence rate is 85 km/Myr [*DeMets*, 2001], if the sediments are transported with the slab, they should arrive in ∼2.4 Myr, thus a signal is expected. The lack of a [10]Be suggest either (1) the sediments are not making it to magma generating depths [*Morris et al.*, 2002; *Carr et al.*, 2007] or (2) the sediment supply is diluted by material from the upper plate through the process of subduction erosion [*Sak et al.*, 2009].

2.4. Onshore Uplift

Onshore studies of Quaternary marine and fluvial terraces along the western margin of Costa Rica document coastal uplift of varying rates along the strike of the MAT [*Sak et al.*, 2009; *Fisher et al*, 2004]. This differential uplift is accommodated by margin-perpendicular normal faults that separate independently behaving blocks [*Fisher et al*, 1998]. Two prominent blocks that stand out along the margins are the Herradura and Esterillos blocks (Figure 1). Although the uplift history of the Herradura block is poorly constrained, it is almost devoid of Tertiary sediments demonstrating an extensive exhumation [*Sak et al*, 2009]. Uplift rates for the adjacent Esterillos block are calculated from Pleistocene marine terraces at ∼3.1–4.0 mm/yr and are some of the highest values in Costa Rica outside the two peninsulas [*Sak et al.*, 2009].

Sak et al. [2009] note that the uplifted portions of the forearc are much wider than the seamounts and the lower slope scallops associated with their passage, calling for either a rigid forearc crust or the off-scraping of seamounts. Although they favor the rigid forearc crust, the lack of sediment cover suggests that long-term continuous uplift is achieved by sediment underplating rather than episodic interaction with under-thrusting seamounts.

3. Data Acquisition

In the spring of 2008, the R/V *Marcus Langseth* acquired the "Osa" line, a 320 km long, trench parallel seismic reflection/refraction transect on the landward side of the MAT offshore Costa Rica as part of the TICO-CAVA (Transects to Investigate the Composition and Origin of the Central Volcanic Arc) project (Figure 1). The transect is ∼90 km from the trench at its northern end and ∼50 km landward of the trench at its southern end. Along this seismic line, 1538 airgun shots from a 6600 cubic inch, 36 gun array were recorded on the R/V *Marcus Langseth's* 8 km long, 636 channel hydrophone streamer at an average shot spacing of 100 m in water depths ranging from 40 to 210 m. The streamer was towed at 6 m depth and the airgun array was also towed at 6 m. Simultaneously, 10 short-period Ocean Bottom Seismometer (OBS) instruments from the Scripps Institute for Oceanography and 16 onshore RefTek seismometers on the Osa and Nicoya Peninsulas recorded refracted arrivals and wide-angle reflection along this seismic line. OBS and RefTek spacing varied between 15–19 km and 6–12 km, respectively.

4. MCS Reflection Data

Multichannel-seismic (MCS) data image acoustic impedance contrasts in the subsurface that result from abrupt changes in velocity or density of the material. Due to the shallow water along this transect, the later arrivals in the MCS data are contaminated by seafloor and basement multiples. We were able to remove much of this noise by applying a low-pass wave-number filter to the shot gathers prior to CMP sorting. Even with this filter, identification of reflections for normal moveout (NMO) velocity analysis was challenging. Following the NMO correction, we applied a spherical divergence correction and stacked the data. After
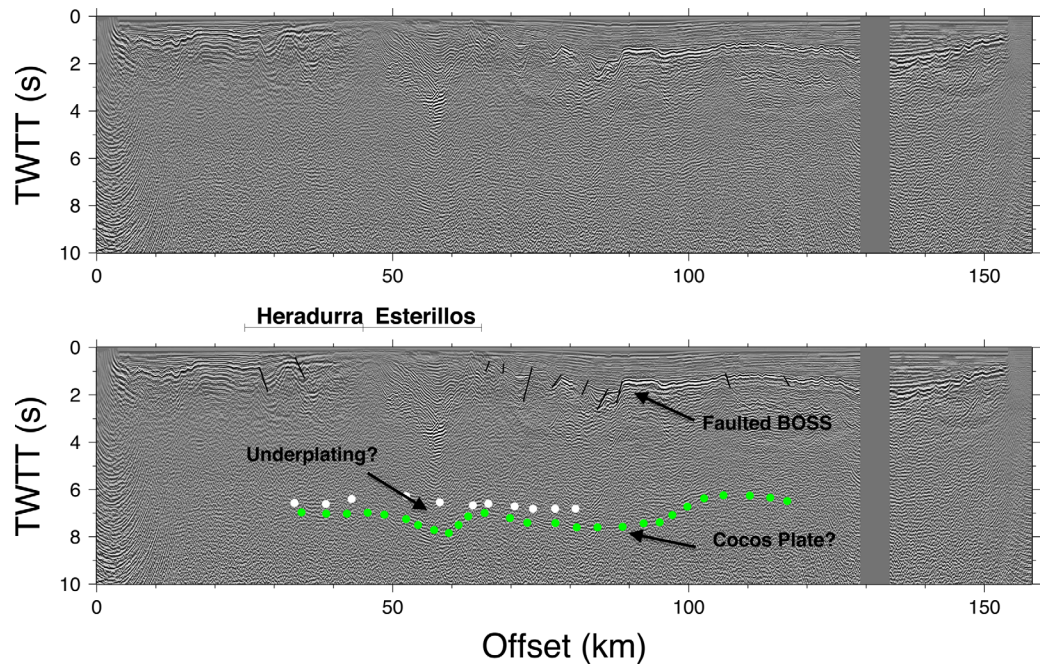
Figure 2. Poststack time-migrated MCS image of the forearc offshore Costa Rica (a) and interpretation (b). Black lines indicate interpreted extensional faults along the BOSS horizon. Green dots indicate the interpreted top of Cocos reflection, white lines indicate upper extent of reflective region interpreted to represent underplated materials beneath the margin wedge. Approximate extent of the Herradura and Esterillos blocks are indicated at the top of the image (projected along direction of convergence).

stacking the data, we applied an f-k migration with a velocity of 2.0 km/s and band-pass filtered the stacked image between 5 and 25 Hz.

The final poststack, time-migrated section (Figure 2) is 160 km long and images the forearc between the Nicoya and Osa peninsulas. It shows complex basement topography marked by a high amplitude reflector commonly observed in the area known as the base of slope-sediments (BOSS) reflector [*Christeson et al.*, 1999]. Notably, the BOSS is cut by numerous high angle faults not seen in dip profiles [e.g., *Hinz et al.*, 1996], consistent with the margin-perpendicular normal faults observed onshore [*Fisher et al*, 1998; *Sak et al.*, 2009]. Underneath the BOSS horizon, near 6–8 s, two-way travel time, a zone of discontinuous reflectivity may represent the Cocos/Caribbean plate boundary along with a significant amount of underplated material (Figure 2b).
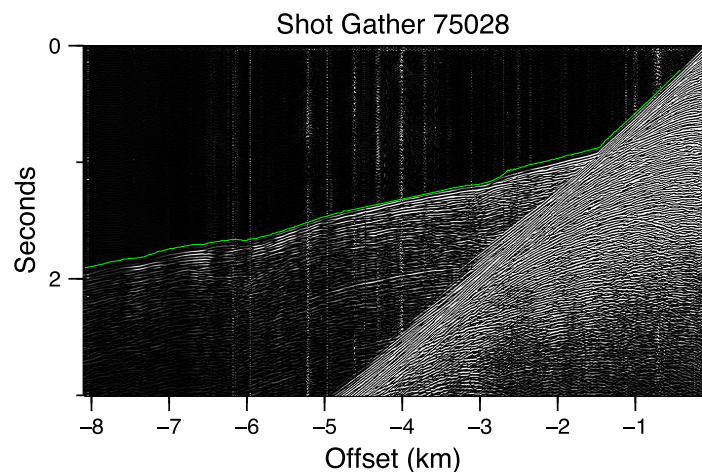

Figure 3. Representative shot gather showing prominent refraction and automatically picked first arrivals (green line) used to constrain the shallow velocity structure.

5. Seismic Velocity Modeling

5.1. MCS Streamer Tomography

The complex topography along the sediment/basement contact observed in the MCS image (Figure 2) is a potential source of uncertainty when modeling crustal velocity structure from wide-angle refraction data. Additionally, the noisy MCS data make it difficult to accurately characterize this boundary across the whole line. Fortunately, due to the shallow water in which the data were
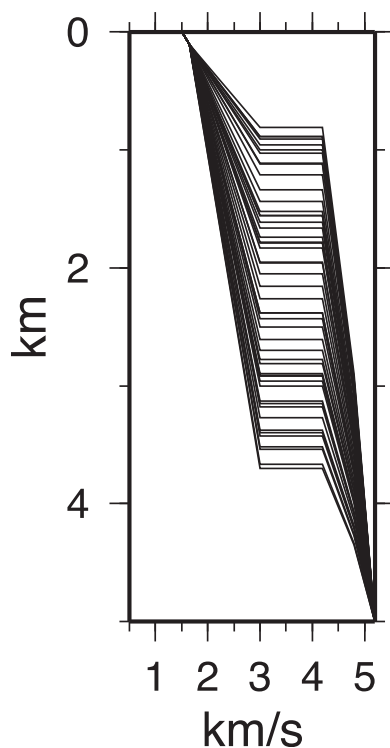
Figure 4. Velocity depth function used as starting models for the Monte Carlo uncertainty analysis performed on the streamer refraction data.

collected, the streamer recorded refracted arrivals over almost its entire 8 km length, providing a unique opportunity to constrain the shallow velocity structure through travel-time tomography.

To facilitate travel time picking, we used an automatic picking algorithm based on *Ramananantoandro and Bernitsas* [1987]. Prior to picking, we applied a band pass filter between 20 and 60 Hz. After applying the automatic picking routine, we manually edited a number of spurious observations and assigned each pick an uncertainty of 0.05 s (Figure 3). Of the 1538 data records, we combined picks from 73 shots, the resulting data set consists of 14,250 first arrival travel-time observations, with an average shot spacing of 2 km.

We use the tomography code described in *Van Avendonk et al.* [1998, 2004] to invert the first arrival travel time observations for shallow velocity structure. The code iteratively traces rays through a velocity model and then updates that model based on the travel-time residuals. The model is parameterized as a grid of velocity nodes spaced 400 m apart in the horizontal and 40 m in the vertical hanging beneath the seafloor. We then try to find a model that best explains the 14,250 travel-time observations under the assumption that the velocity field is smoothly varying in space.

Tomographic velocity reconstructions are nonunique and may depend on the starting model chosen for the inversion. We adopt a Monte-Carlo approach to assess the dependency of our final model on the starting model. Because we expect a sharp velocity contrast between the slope sediments and the underlying basement, we chose to include a sharp velocity contrast in our starting models. We define 50 starting models that have a velocity of 1.65 km/s at the top of the sediments and increase to 3.0 km/s at some depth where the velocity increases sharply to 4.2 km/s (Figure 4). The depth to the discontinuity for each model was determined by drawing from a uniform, random distribution between 0.75 and 3.75 km. For each starting model, we iterated raytracing and regularized inversion steps until a minimum RMS misfit was achieved.

A representative model (Figure 5a) has an RMS misfit of 0.053 s and a reduced χ^2 value of 1.05; travel-time fits are shown in Figure 5c. The standard deviation for each model parameter (Figure 5b) gives an estimate of the uncertainty in the solution. Standard deviations, where rays traverse the model (Figure 5d), are generally less than 0.1 km/s except for between x = 0 and x = 40, where they average 0.7 km/s. The structure in this region is likely too complex for the data to resolve.

When converted to time, the velocity model the velocity model shows a similar structure as the stacked MCS image (Figure 6). The 3.5 km/s contour closely follows the BOSS horizon across much of the model except between x = 0 and 40 km, where the MCS image depicts the largest lateral variations in structure.
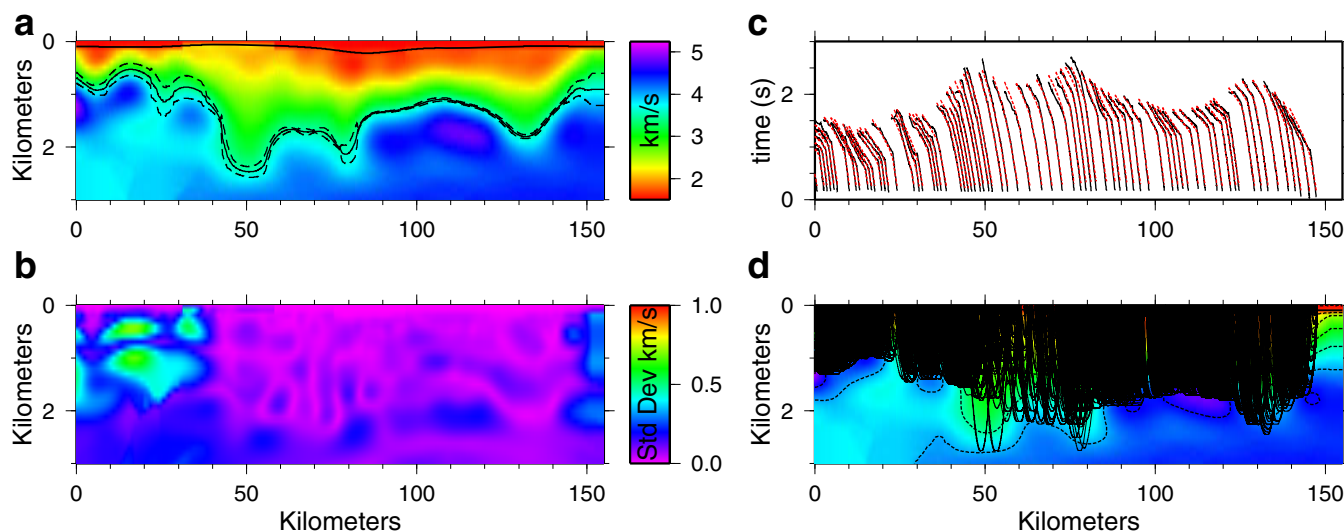
5.2. Wide-Angle Seismic Data
Wide-angle seismic data were collected to constraint the velocity structure of the margin wedge and the subducting Cocos plate. The OBS instruments recorded three orthogonal components and a hydrophone. In general, we find the highest signal to noise ratio on the z-component; the exception to this is OBS-1 where the hydrophone contains significantly better data. Due to the shallow water and careful shipboard navigation during OBS operations, relocation of the instruments on the seafloor was not necessary. We apply a reduction velocity of 6 km/s to each OBS/RefTek instrument, band pass filter the data (3–12 Hz), and apply an automatic gain control to aid in interpretation. The quality of the OBS records is a function of water depth, with the highest signal to noise ratios observed on the deepest instruments. Out of the 16 RefTek

Figure 5. Streamer tomography results showing one model realization (a) standard deviation for all 50 models (b), travel time fits (c), and raypaths (d). Solid black line in Figure 5a indicated the average 3.5 km/s contour and dashed lines show the standard deviations. This is the boundary used to represent the sediment/basement interface in the wide angle models shown in Figures 8 and 9. Vertical exaggeration is 15:1.

land stations, 8 of the instruments from the Nicoya peninsula had signal to noise ratios high enough to interpret Osa peninsula instruments were too noisy to interpret. Figure 7 shows eight representative data records.

We identify four refraction phases, which we interpret as rays turning within the sediment layer, an upper and lower margin wedge, and the upper oceanic mantle. We observe reflections off of the oceanic Moho (Pmp) on most of the instruments as well as four shallower reflections (Figure 7, NP-9, OBS 5, and OBS 6), which we cannot confidently interpret. We assign travel-time uncertainties, which are generally a function of offset and range from 0.05 s in the nearest offsets to 0.12 at the largest offsets. Our phase interpretation is shown in Figure 7, phase terminology and model fit statistics are summarized in Table 1.

We model the wide-angle arrivals using RAYINVR [*Zelt and Smith*, 1992], a modeling code that traces rays through a sparsely parameterized velocity structure and allows both forward and inverse modeling approaches Model parameter uncertainties can be estimated with the following procedure [*Zelt and Smith*, 1992]: (1) perturb a model parameter from the final model, (2) fix the perturbed parameter and try to fit the data by inverting for neighboring parameters. The largest perturbation for which the data can be fit as well
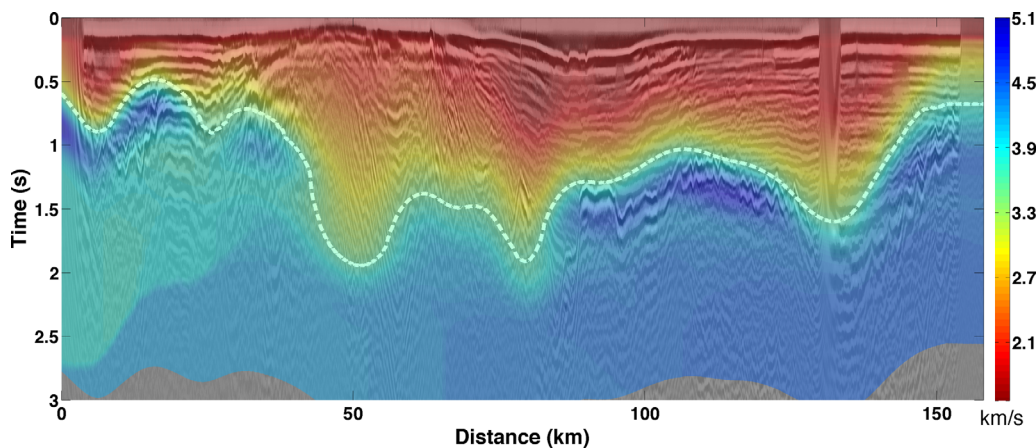
Figure 6. Streamer tomography model from Figure 5a overlaid on the MCS image shown in Figure 2. White-dashed line shows the average location of the 3.5 km/s contour interpreted to represent the depth to basement in wide-angle models (Figures 8 and 9).

Table 1. Event Terminology and Model Fit Statistics[a]

Event	Event Type	Ndata	Assigned Uncertainty (s)	RMS Misfit (s)	Reduced Chi Square
Ps	Refraction, sediments	329	0.03	0.044	2.173
Pumw	Refraction, upper margin wedge	1481	0.05	0.129	6.052
Plmw	Refraction, lower margin wedge	2909	0.08	0.102	1.620
Pmmw	Reflection, top of lower margin wedge	38	0.093	0.08	1.189
Pn	Refraction, upper mantle	75	0.12	0.229	2.353
		75*		0.270	3.295
Pbmw	Reflection, Top of Cocos plate	215	0.10	0.075	0.455
		158*		0.08*	0.452*
O2-3	Reflection, oceanic layer 2/3 boundary	60*	0.10	0.108*	0.828*
Pmp	Reflection, oceanic Moho	928	0.10	0.136	1.285
		928*		0.136*	1.285*

[a]Numbers marked with an asterisk refer to Model 2 (two-layered Cocos plate).

as in the final model, determined by and F-test, is the estimated uncertainty. Model uncertainties are summarized in Table 2.

In the following sections, we provide an in-depth discussion of our data interpretation and modeling procedure, which gives rise to two possible models (Figures 8 and 9).

5.2.1. Margin Wedge

The OBS and RefTek records show a prominent branch of arrivals with an apparent velocity of ∼4.5 km/s from about 15–70 km offset. On OBS instruments 5, 6, 7, and 9, this branch contains a bowtie triplication indicating a velocity discontinuity (Figure 7). On these instruments, we use the triplication to differentiate between arrivals that sample the upper portion of the margin wedge (Pumw) and those that travel deeper into the lower margin wedge (Plmw).

We define the depth to the top of the margin wedge by averaging depths 3.5 km/s contour from the 50 streamer models. Between 0 and 160 km, the velocities in the upper margin wedge are 4.5 $\pm$3 km/s except for between x =∼60–80 km where 3.4 km/s provides the best fit to the data. Although we have trouble fitting the observed travel times for this phase on OBS-5 (RMS misfit for just OBS-5 is 0.165 m/s), our uncertainty analysis suggests that velocities greater than 3.5 km/s do not fit the data as well, while the velocity could be as low as low as 3.3 km/s. The streamer tomography results to not reveal a significant velocity reduction in this area and it is possible that the poor data fit for OBS-5 is due to unresolved structure along the sediment/basement interface.

Table 2. Model Uncertainty Summary[a]

Parameter	Model Offsets (km)	Uncertainty (+/-)
Sediment velocity	0 < x < 40	*0.7 km/s
	40 < x < 160	*0.1 km/s
Sediment thickness	0 < x < 20	*0.15 km
	20 < x < 50	*0.3 km
	50 < x < 160	*0.05km
Upper margin wedge velocity	x < 0	Not constrained
	0 < x < 60	0.3 km/s
	60 < x < 80	0.15 km/s
	80 < x < 160	0.3 km/s
Lower margin wedge velocity	x < 30	Not constrained
	30 < x < 70	0.3 km/s
	70 < x < 160	0.2 km/s
Upper margin wedge thickness	x < 50	Poorly constrained
	50 < x < 160	0.5 km
Lower margin wedge thickness	x<-20	Not constrained
	−20 < x < 0	0.5 km
	0 < x < 160	Uncertain, depends on phase interpretation
Cocos plate velocity		Poorly constrained
Moho depth		5 km, depends on Cocos Plate structure

[a]Uncertainties were determined using an F-test as outlined in *Zelt and Smith* [1992]. Asterisks denote statistics determined from Monte Carlo analysis on streamer refraction data.

At model distances greater than 55 km, it is clear that the boundary between the upper and lower margin wedge is marked by a velocity discontinuity. Here we find the data are best fit by a velocity jump of 0.6 km/s (Figure 10) across a boundary that shallows to the southeast (increasing model distances). Along the top of the lower margin wedge, at model distances greater than 55 km, velocities increase from 5.6 km to 6 km/s are constrained to with 0.1 km/s. At distances less than 55 km, a small (<0.2 km/s) contrast across this boundary is not constrained by the data.

The thickness of the upper margin wedge ranges from 2 km at the southeastern end of the line to ∼4.5 km at model distance 60 km. It is constrained by the crossover point between Pumw and Plmw as well as one reflection event (Pmmw), which we observe on OBS 5 (Figure 7).

We observe Plmw at source-receiver offsets greater that 80 km on several of the RefTek instruments. Although we lack reverse ray coverage for these observations, a velocity of 6.7 km/s is required near the base of the lower margin −40 and 20 km; we cannot fit these arrivals with velocities less than 6.6 km/s.
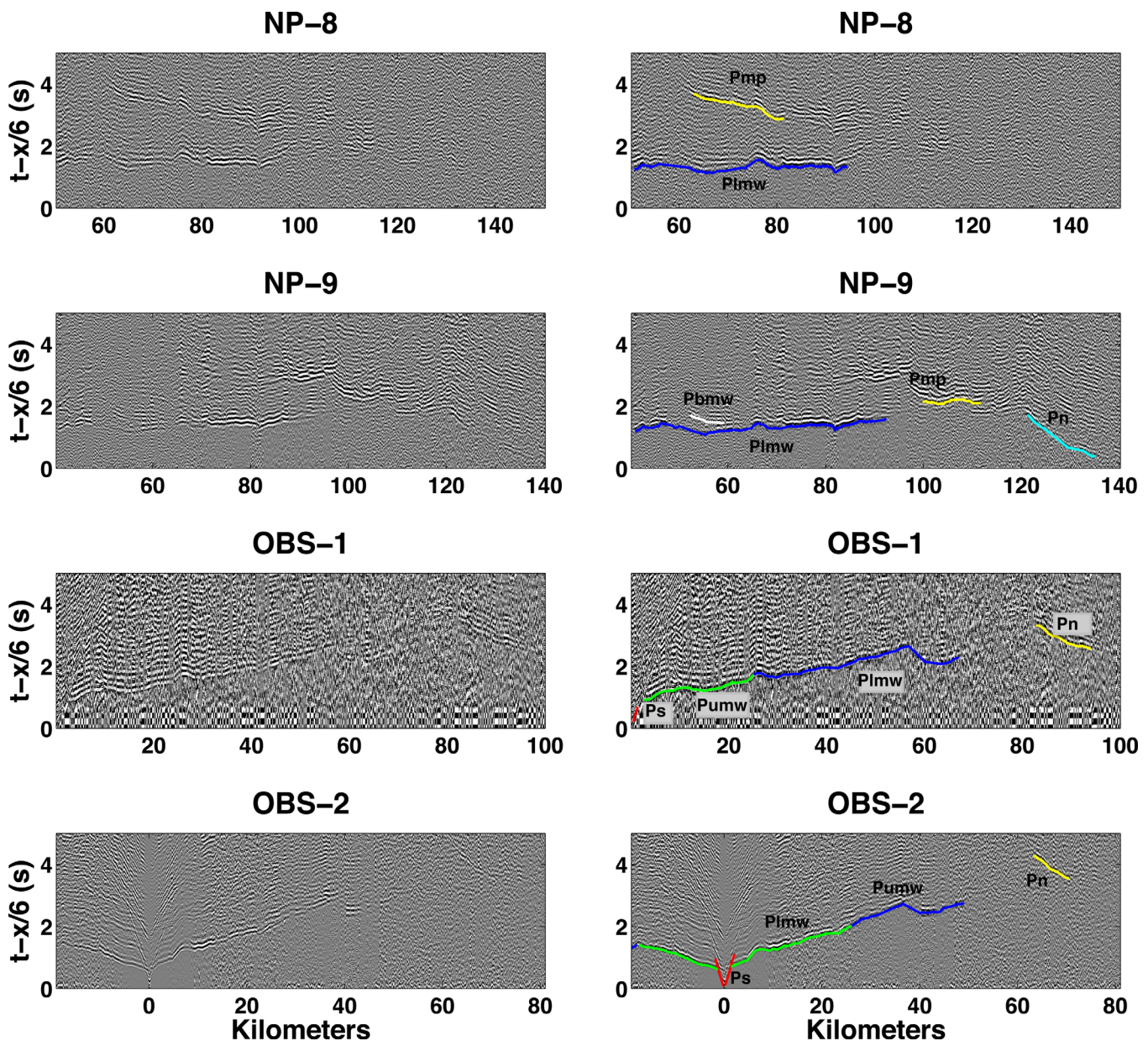

Figure 7. Representative data records (left column) and interpretations (right column).
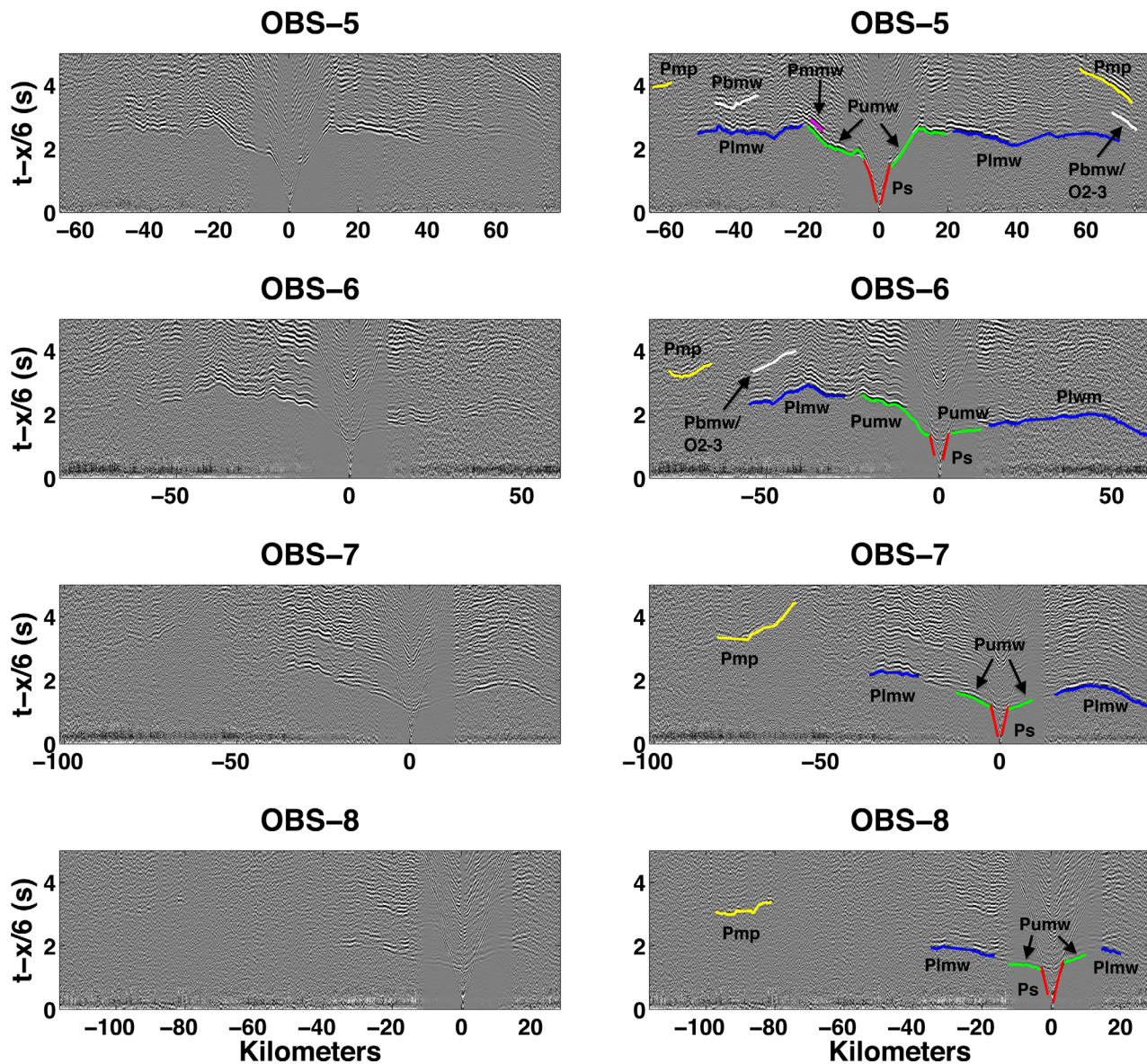
Figure 7. Continued

Depth to the bottom of the lower margin wedge is constrained by reflections on NP-9 and OBS 5 (Figure 7), which we are confident in interpreting as the top of the Cocos plate. Given the velocity structure indicated by fitting long offset Plmw phases, the reflection observed on NP 9 lies at ~14.6 ± 0.5 km depth between x = −20 and x= 0. Between x = 40 and x= 60, the reflection observed on OBS 5 constrains the top of the Cocos plate to 17.4 ± 0.5 km, though the velocities near the bottom of the lower margin wedge are not as well constrained here.

The modeled depth of these reflections are consistent with the depth to the Cocos plate as modeled by a previous studies in this area [*Ye et al.*, 1996; *Christeson et al.*, 1999; *Zhu et al.*, 2009], thus we feel confident of our interpretations. Based on the Cocos plate velocity structure presented in these studies and the 6.7 km/s velocity in the lower margin wedge that we observe, we expect a velocity inversion across the Cocos/Caribbean plate boundary. However, including a velocity inversion across this boundary limits the range of offsets that we can trace rays through the lower margin wedge to. Given the geometry of our data set, which runs along-strike of a dipping structure, and previous observations that suggest that velocities in the lower margin wedge increase landward [*Ye et al.*, 1996; *Christeson et al.*, 1999; *Zhu et al.*, 2009], this difficulty can be explained by out of plane structure. First arrivals are likely to traverse deeper portions of the margin
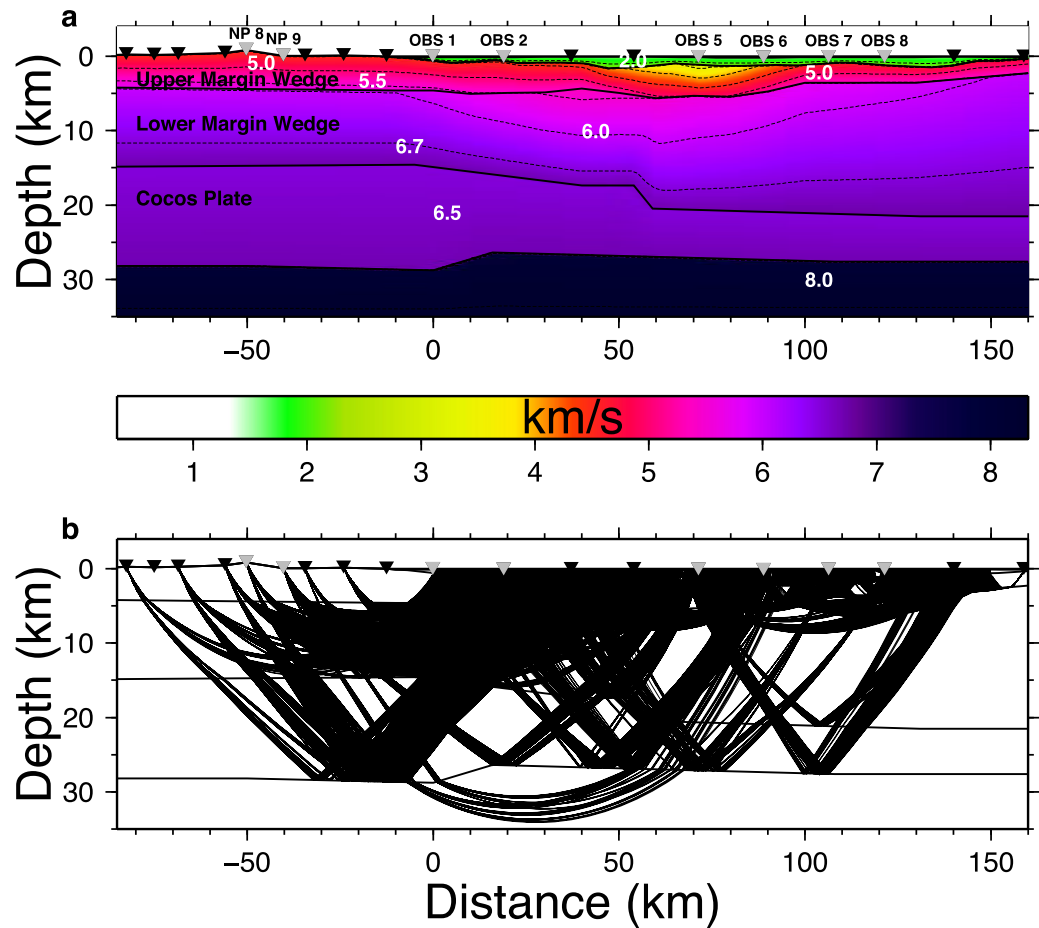
Figure 8. Model 1 velocity model (a) and ray coverage (b). This model assumes that all of the weak reflecting events observed on NP 09, OBS 5, and OBS 6 represent the top of the Cocos plate (Figure 7). The final RMS misfit for this model is 0.115 s and reduced $\chi^2 = 3.194$.

wedge, which lie landward of and out of the plane of our model, while reflecting phases likely travel seaward and out of the plane of our model and sample a shallower portion of the subducting Cocos plate.
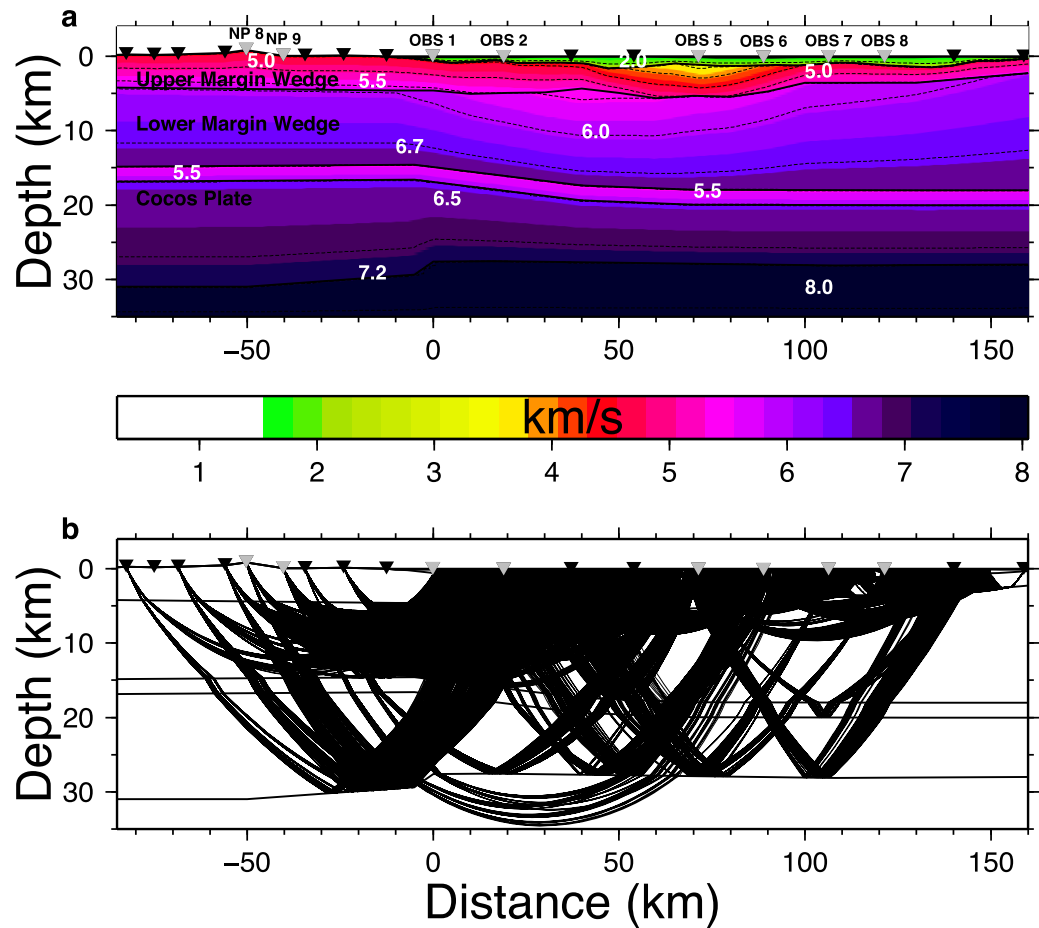
5.2.2. Cocos Plate

In addition to the two reflections discussed above, we observe two more reflections (Figure 7, OBS 5 and OBS 6) that possibly originate from the top of or within the Cocos plate. Interpreting these reflections as the top of the Cocos plate results in a significant deepening of the Cocos plate toward the southeast, while interpreting them as events from the transition between oceanic layers 2 and 3 within the Cocos plate results in a less severe lateral change in structure. Because we cannot confidently differentiate between these two cases, we present both models. In the first model, we treat all of the observed reflections as the top of the Cocos plate (Pbmw) and in the second model we interpret two of the reflection as the top of the Cocos plate and two as the oceanic layer 2/3 boundary (02-3).

5.2.2.1. Model 1

In this model, we assume that the two ambiguous reflections occur at the plate boundary. This causes the top of the Cocos plate to have significant topography near model-offset 55 km, directly inboard of the seamount segment. We next estimate the depth to the Moho and average velocity structure of the Cocos plate by assigning a fixed velocity to the plate and solving for Moho depth using PmP and Pn arrivals. We do this for a range of velocities and choose the model with the lowest RMS misfit (Figure 11). The final model (Figure 8a) has the Cocos plate ranging from 6 km thick in the southeast part of the model up to 14 km beneath the Nicoya peninsula with an average velocity of 6.6 km/s. It has an RMS misfit of 0.115 s and a reduced χ^2 value of 3.194.

The amount of relief along the plate boundary for this model (4 km over a distance of 5 km) is not unlikely given the amount of relief observed on the "seamount" segment immediately seaward of this portion of the model.

Figure 9. Model 2 velocity structure (a) and ray coverage (b). This model assumes that the shallowest of the weak reflecting events represent the top of the Cocos plate. We then use the velocity structure reported in *Ye et al.* [1996] for the Cocos plate and find that the remaining reflections agree with the oceanic layer 2/3 boundary. The final RMS misfit for this model is 0.114 s and reduced $\chi^2 = 2.927$.

5.2.2.2. Model 2

In this model, we assume that two ambiguous reflections represent the boundary between oceanic layers 2 and 3. We model the top of the Cocos plate out to model offset 50 km in the same way as the previous model, but extend the top of the Cocos plate to the southeastern edge of the model at a depth of 18 km. We assume the Cocos plate has a similar velocity structure to that reported by *Ye et al.* [1996] and find that the remaining reflections agree with a 2 km thick, 5.5–6.0 km/s oceanic layer 2. Assuming that oceanic layer 3 has a velocity that increases from 6.5 to 7.2 km/s, we model Moho depths with Pmp and Pn arrivals. The faster velocities in the lower Cocos plot (compared to Model 1) predict a much deeper Moho (Figure 9a) and Cocos plate that is 16 km thick beneath Nicoya peninsula and 8 km thick on the southeastern portion of the line. The RMS misfit and reduced χ^2 values for this model are nearly identical to the previous model, 0.114 seconds and 2.927; travel-time fits for several representative instruments are shown in Figure 12.

5.2.3. Model Resolution

Above the Cocos plate, both the structure of our models is identical (except for variations in the depth to the Cocos plate). Regions with reverse raypath coverage (between 0 and 160 km) are generally more well-constrained than regions where all rays travel in the same direction (model distances less than 0). Resolution estimates for each velocity parameter, generated by RAYINVR's dmplstsqr routine, indicate velocities are well resolved in the upper and lower margin wedge between model distances 0 and 140 whereas Cocos plate structure is poorly resolved (Figure 13). Although we are unable to constrain Cocos plate structure, the deepening of the oceanic Moho beneath Nicoya Peninsula is a robust observation. Although Moho depth varies by several kilometers depending on the velocity structure chosen, in both models, the Moho deepens toward the northwest end of the line.
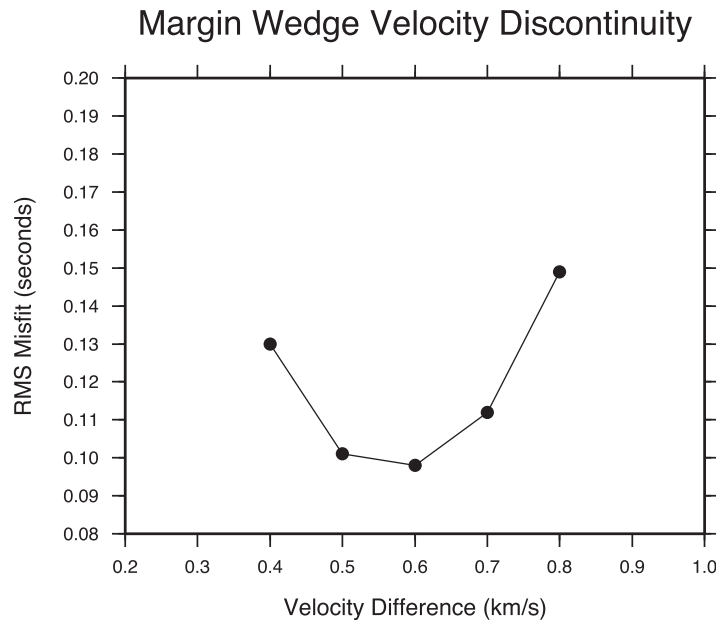
Figure 10. RMS misfit versus velocity discontinuity magnitude across the upper and lower margin wedge for model distances greater than 55 km. A discontinuity of 0.6 km/s provides the best fit to the data.
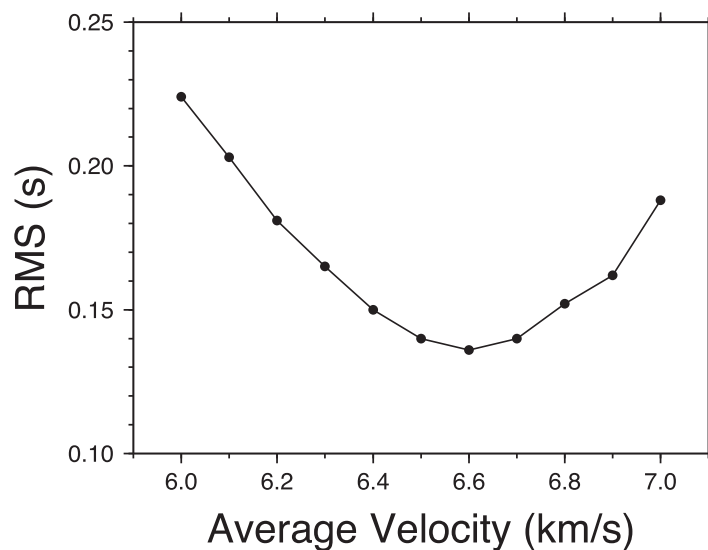
5.2.4. Reflectivity Zone

The MCS image along the Osa line shows a weak band of discontinuous reflections with two-way travel-ties between 6 and 8 s (Figure 2). We use RAYINVR to model these travel-times as reflectors floating with our velocity model. Since the velocity structure of models 1 and 2 are the same for the upper 15 km, and since model 2 seems to be most consistent with the data given the weak reflection observed on OBS-5, we use model 2 to perform this analysis.

The results of this modeling show that the latest arriving events correspond to the top of the Cocos plate, while the earlier events lie up to 3.5 km shallower than this (Figure 14a). The accuracy of these depths is strongly dependent on the accuracy of the velocity model; however, it is unlikely that the earliest events lie near the top of the Cocos plate. To verify that these reflectors are above the slab, we vary the velocity within the lower margin and find that, due to the longer ray paths, the wide-angle reflections are much more sensitive to velocity variations than the normal incidence reflections in the MCS image.
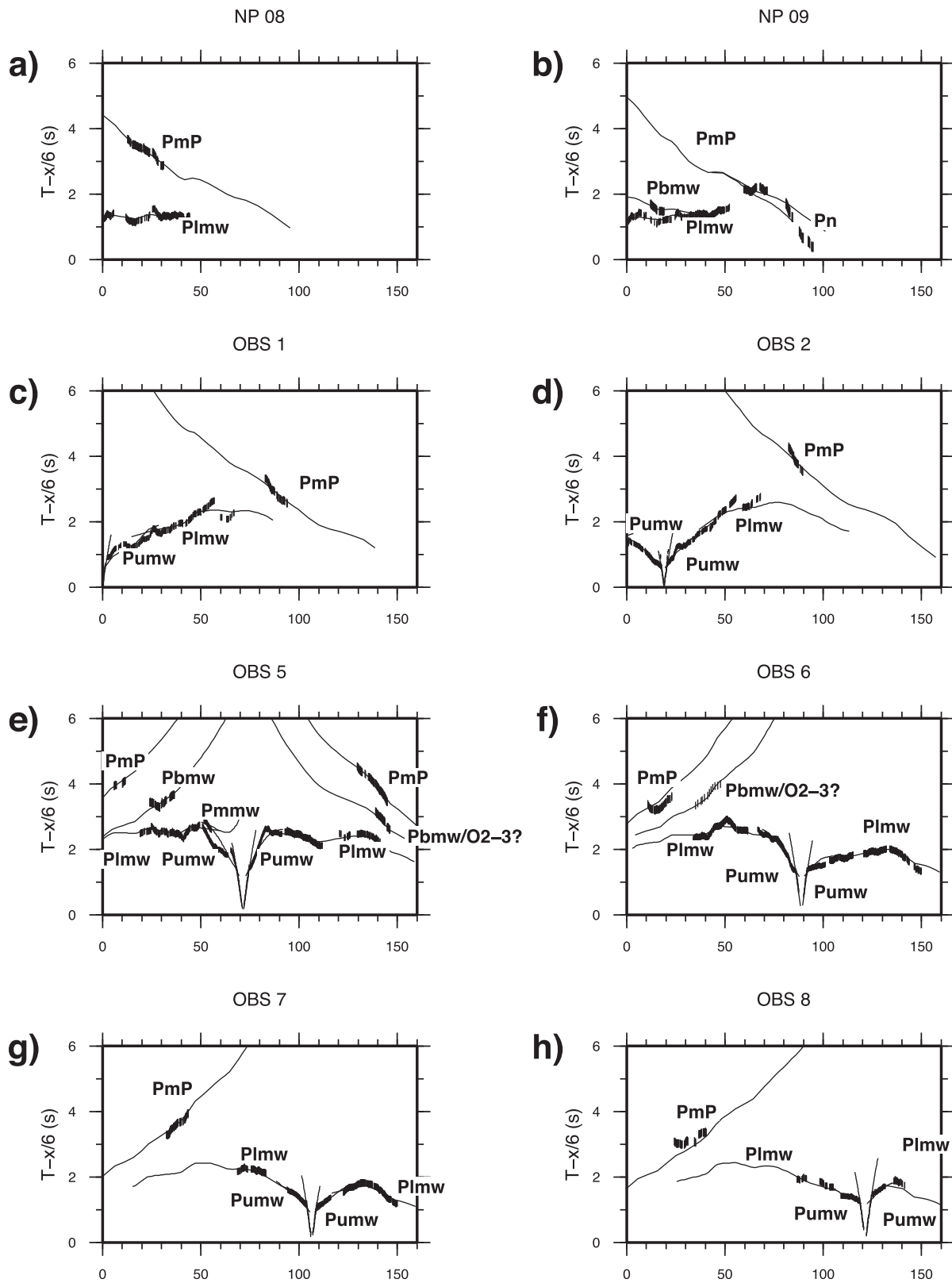
6. Discussion

The seismic results presented in this paper image forearc structure offshore Costa Rica. The primary boundaries that we image are the BOSS horizon, the Caribbean/Cocos plate boundary, and the oceanic Moho. The most robust observations that our data allow us to make are (1) margin perpendicular extensional faulting of the BOSS horizon, (2) The deepening of the oceanic Moho beneath Nicoya Peninsula, and a reflective zone near the Cocos/Caribbean plate boundary that is spatially correlated with onshore uplift observed along the coast. In the following discussion, we first compare our wide angle velocity model to previous studies in the area and then we argue that faulting of the BOSS horizon combined with the reflective area near the Cocos/Caribbean plate boundary provide evidence for underplating beneath the inner forearc.


Figure 11. RMS misfit for Pmp and Pn arrivals versus average velocity of the Cocos plate. The minimum RMS of 0.136 corresponds to an average Cocos plate velocity of 6.6 km/s.

Figure 12. Predicted travel times (solid lines) and observed travel times (black lines) for the instruments shown in Figure 5. The size of the black lines indicate the assigned uncertainty. Since the predicted travel time curves for both models are virtually identical, only those for model 2 are shown.
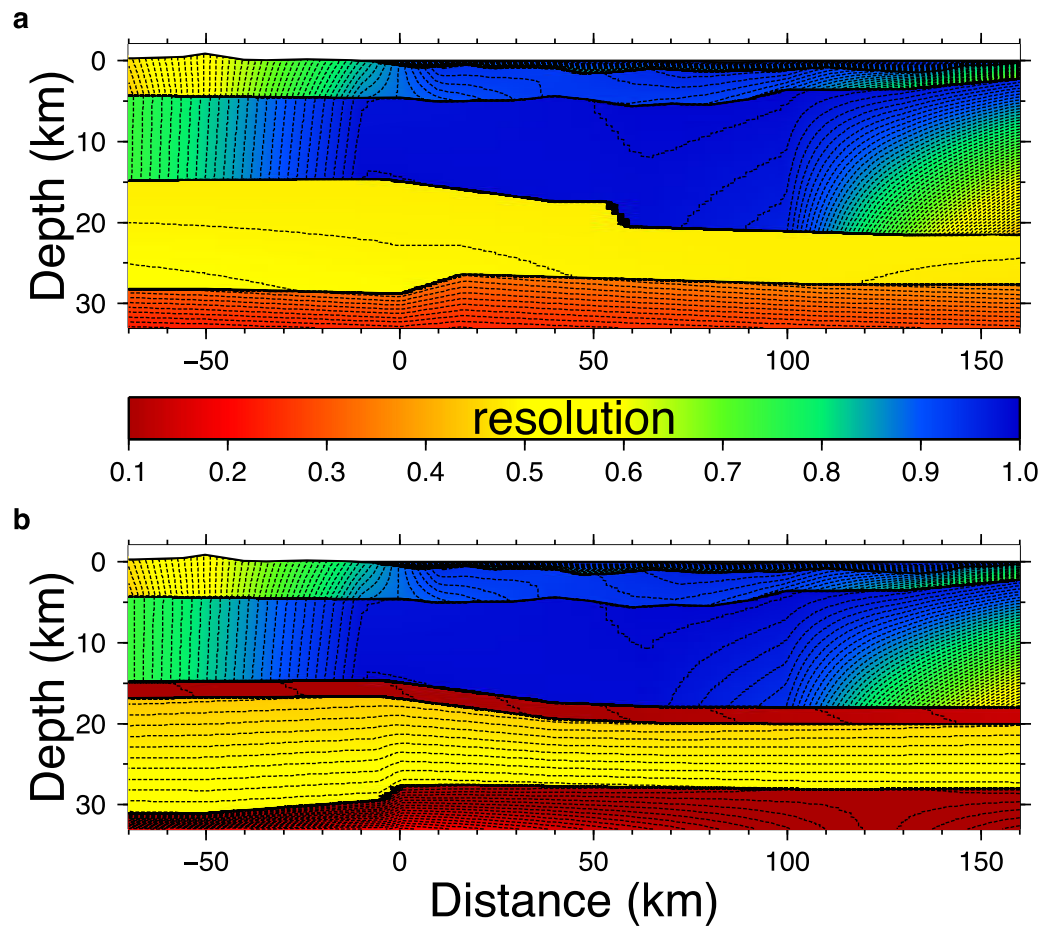
Figure 13. Resolution estimates for Model 1 (a) and Model 2 (b). These estimates are the diagonal elements of the resolution matrix calculated by RAYINVR's dmplstsqr routine. Values greater than 0.5 are considered well resolved.

6.1. Comparison to Other Models

Christeson et al. [1999] present a model that extends from ∼20 km seaward of the trench onto the Nicoya Peninsula (Figure 1, Line 101). Their model shows a two layer Cocos plate subducting beneath a margin wedge that thickens and increases in velocity towards the coast. Beneath Nicoya Peninsula the margin wedge consists of three layers and increases in velocity from 4.2 km/s near the surface, to 6.95 km/s near the top of the Cocos plate. Beneath Nicoya Peninsula, the 5 km thick, EPR derived Cocos plate ranges from ∼14 km to greater than 25 km depth. At the approximate location of the Osa line, it is ∼20 km beneath the sea-surface. A thin low velocity layer between the Cocos and Caribbean plate persists to the greatest depths modeled.

Ye et al. [1996] present three dip lines and one along-strike line. One of their dip lines (Line 200, Figure 1), traverses from ∼30 km seaward of the trench onto the coast. This line is perpendicular to the Osa line and intersects it near OBS 3. This model shows a two-layer margin wedge with velocities increasing landward and with depth. Near where the Osa line intersects this model, just beneath the sediments the upper margin wedge has a velocity of 5.1 km/s ∼increasing to 6.0 km/s at ∼10 km depth where a 0.4 km/s discontinuity marks the top of the lower margin wedge. Although their model shows the lower margin wedge having a velocity of 6.6 km/s near the top of the Cocos plate, the authors report that only the upper portion of this layer is constrained by their data. An ∼1.5–2 km thick, low velocity layer runs along the top of the 6–7 km thick, CNS-2 derived Cocos plate. Another line (Line 300, Figure 1) shows a similar thickness in the CNS-1 derived Cocos plate. Their strike line (Line 100) is trenchward of the Osa line, shows a one layer margin wedge 4.9 km/s at the top and 5.5 km/s at the bottom and decreasing in thickness from ∼12 km in the northwest to ∼9–10 km in the southeast. A 7–8 km thick, 2 layer Cocos plate thickens slightly to the SE while the oceanic Moho shallows.
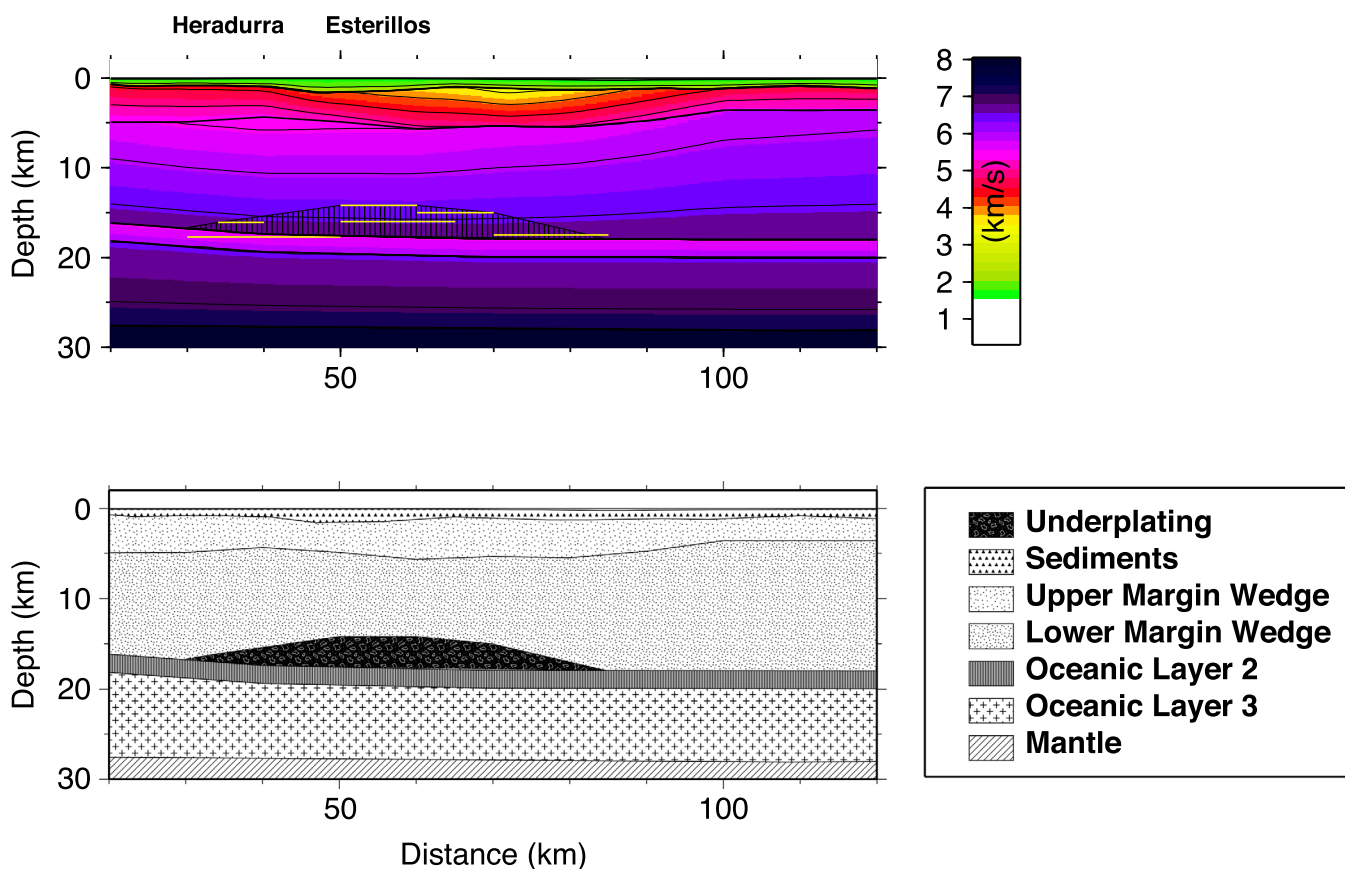
Figure 14. Results of modeling the MCS reflections through the velocity model derived from wide angle data (a) and geologic interpretation (b). The yellow lines represent floating reflectors, the hatched area represents the inferred region of underplating. The projected locations of the Herradura and Esterillos blocks are also shown. Shape of the underplating in Figure 14b is interpreted and not constrained by the data.

Zhu et al. [2009] present two dip lines and two strike lines that are seaward of the Osa line, southwest of OBS's 5, 6, and 7 (Figure 1). Their dip lines both show a two-layer margin wedge with an upper layer of 4.2–5.3 km/s and a lower layer of 5.5–6.1 km/s. Like the previous models, margin wedge velocities increase landward. Their strike lines show that the lower margin wedge thins to the southeast. A low velocity layer of variable thickness sits between the Cocos and Caribbean plates and they image a "mega-lens" ∼30 km inboard of the trench and 4–6 km beneath the sea surface. The note that the "mega-lens" is bound beneath by a low-velocity zone, and interpret this as evidence for fluid drainage along the top of the 6–7 km thick Cocos plate.

Like the previous models, our models show a two-layer margin wedge overlying the Cocos plate. The primary differences between our models and previous studies are (1) a reduction in upper margin wedge velocities between model distances 60 and 80 km, (2) a margin wedge that thickens to the SE and has a higher velocity than previously reported, and (3) a Cocos plate that thickens to the NE.

The upper margin wedge in our models is 2–5 km thick and has a velocity of 4.5–4.7 km/s beneath the slope sediments except for the region between x= 60 to x=80 km (Figures 8 and 9). Here a velocity of 3.4 km/s best fits the data from OBS-5. This is a lower velocity than any of the previous studies report for the upper margin wedge and it is not supported by our streamer tomography results. Although this lower velocity may be due to poorly resolved topography along the BOSS horizon, it could also reflect a higher frequency of faults in the area. Our MCS image, although difficult to interpret, appears to show more faulting in this region (Figure 2). The streamer data may not require this low velocity since the data are restricted to source receiver offsets that are less than 8 km. The longer travel-paths from the OBS data likely encounter a larger number of faults and therefore accumulate larger travel-time delays.

As a whole, it is difficult to determine whether the models from the previous studies we cite provide evidence for any along-strike variations in the margin wedge thickness. The models of *Zhu et al.* [2009] do not

extend far enough landward to compare them to the models of *Christeson et al.* [1999] and *Ye et al.* [1996]. *Ye et al.* [1996] do present one strike line that shows the margin wedge thinning to the SE; however, this line is not parallel to the trench and gets closer to the trench toward the southeast (Figure 1, Line 100), thus the apparent thinning of the margin wedge that they show may only reflect the geometry of their survey and not that of the margin wedge. Our models suffer from poor ray-coverage (Figure 8b and 9b) in the lower margin wedge at models distances greater than ∼50 km. Additionally, our modeled depths to the Cocos plate in this region depend on the manner in which we interpret the few reflections that we observe from this region. Given the poor constraints in this region of the model, we cannot say for certain how the thickness of the margin wedge changes towards the SE. Lower velocities in the lower margin wedge would decrease the depth to the top of the Cocos plate.

We report higher velocities in the lower margin wedge than any of the previous studies. Beneath Nicoya Peninsula, our model is constrained at 6.7 ± 0.1 km/s by nonreversed raypaths. Given that all of the previous studies report velocities that increase landward and that the Osa line is farther from the trench than most of these studies, we think that these velocities are likely to be representative of the lower margin wedge.

Finally, both of our models depict a Cocos plate that thickens to the NE and an oceanic Moho that deepens in the same direction both trends that are not evident in the previously published models. Given that our data do not constrain the velocity structure of the Cocos plate, it is difficult to determine whether the thickening of the Cocos plate and the deepening of the Moho beneath Nicoya peninsula are real, or whether they are representative of changing velocity structure. It is notable that the Cocos plate begins to thicken at the approximate transition between CNS-1 and CNS-2 crust. An offshore survey that traversed this transition reported an 8–9 km thick CNS-1 crust with a low velocity body in the lower oceanic crust [*Van Avendonk et al*, 2011]. If such a low-velocity body exists beneath the Osa line, it would explain why our model shows a thickness of 14 km here. Lower velocities would not require is much thickness to explain the delayed travel-times.

On the southeast part of the Osa line, our model does not show the expected thickening of the Cocos plate associated with the Cocos ridge. The most likely explanation for this is that our data do not sample the Cocos ridge. The southeasternmost Pmp observations that we make reflect off the Moho at model distance near 100 km, beneath OBS 7 (Figure 8b and 9b). This corresponds to the northeastern flank of the Cocos ridge. Our data likely miss the thicker crust of the Cocos ridge.

6.2. The BOSS Horizon

The extent of the BOSS horizon has been extensively documented through the lower to middle continental slope [e.g., *Ye et al.*, 1996; *Christeson et al.*, 1999; *Meschede et al.*, 1999; *Vannucchi et al.*, 2001]. *Meschede et al.* [1999] interpreted the prevalence of trench-parallel extensional faulting to be the result of subsidence related to tectonic erosion. Further support of this interpretation comes from the results of ODP Leg 170, which penetrated the BOSS horizon ∼7 km landward of the trench at Site 1042 and found 16-17 a carbonate breccias with a fossil assemblage consistent with a mid to upper slope depositional environment, indicating substantial subsidence of the forearc [*Vannucchi et al.*, 2001]. Notably, dip lines extending from the outer margin wedge up to the shelf region show that the BOSS horizon transitions from a rough to a smooth reflection at the shelf [*Hinz et al.*, 1996]. Beneath the shelf, margin parallel faulting is not observed.

We image the BOSS along the upper shelf of the Costa Rican margin as a mostly continuous feature, frequently interrupted by what appear to be margin perpendicular extensional faults (Figure 2). These faults can be traced onshore to the small-scale boundaries observed by *Fisher et al.* [1998] and attributed to differential rates of Quaternary uplift along the margin possibly associated with the underplating of seamounts beneath the inner forearc. To reconcile inner-arc uplift with long-term subsidence of the outer forearc recorded in the BOSS horizon, we suggest that sediments, seamounts, and tectonically eroded material from the outer forearc are underplated beneath the inner forearc. This process could explain both the observed uplift and the lack of [10]Be signature observed lavas along the Costa Rican portion of the arc.

6.3. Plate Boundary

A commonly observed feature at erosive convergent margins is a layer between the upper and lower plates that likely consists of fluid-rich sediments and material removed from the upper plate. Sometimes referred to as the Subduction Channel. [e.g., *Vannucchi et al.*, 2012; *Shreve and Cloos*, 1986], this feature is widely observed in reflection images offshore Costa Rica and is recognized as a characteristic bifurcation of the

plate boundary reflection [*Ranero and von Huene*, 2000; *Zhu et al.*, 2009] and has been imaged at depths reaching 12 km [*Ye et al.*, 1996].

At Costa Rica, the majority of the sediments arriving at the trench are being subducted and a significant amount of the overriding plate is removed over time through the process of subduction erosion [*Meschede et al.*, 1999; *Vannucchi et al.*, 2001; *von Huene et al.*, 2004]. In order to account for these processes, there must be a significant amount of mass being transported along the plate boundary. Previous studies of the Costa Rican forearc have modeled a low-velocity layer of varying thicknesses and landward increasing velocity to depths approaching 15 km [*Ye et al.*, 1996; *Christeson et al.*, 1999; *Zhu et al.*, 2009]. Since velocity modeling is heavily dependent on modeling first arrival times, low-velocity layers are difficult to resolve. *Ye et al.* [1996] argued for the existence of this low-velocity zone based on the observed high amplitude reflections, which would require a higher velocity contrast across the plate interface than the first arrivals would indicate. Their low velocity zone varies from 0.4 to 1.0 km in thickness assuming a velocity of 3.0 km/s and fits their observed travel-times better than introducing a high velocity layer across the interface. *Christeson et al.*, [1999] also report that a low-velocity zone of 0–200 m thickness is required to produce a geologically reasonable model and *Zhu et al.*, [2009] model reflections from both the top and the bottom of the subduction channel and adjust the thickness and velocity as required by the travel times. Their final model shows a 1.0–1.5 km thick "mega-lens" around 30 km landward of the trench that decreases in thickness toward the arc. Thus, there is a large body of evidence in support of a subduction channel beneath Costa Rica along which sediments and tectonically eroded material are being transported to some depth within the subduction zone.

The nature of the plate boundary at depth has important implications for understanding the transport of material to depth within the subduction zone and the ultimate fate of incoming sediments. Although the wide-angle data on the Osa line do not indicate the presence of a subduction channel, the reflection image shows a band of discontinuous reflections with two-way travel-times that are consistent with the depth to this interface as constrained by the wide-angle data. Modeling the reflections observed in the MCS indicate that a reflective region roughly 40 km wide and 1–3 km thick sits directly above the Cocos plate beneath the Herradura and Esterillos blocks (Figure14), which record some of the fastest Quaternary uplift rates in Costa Rica, not including the Nicoya and Osa peninsulas. The thickness of this body is many times greater than the thickness of the incoming sediments, which when compaction and fluid loss is considered, indicates a steady growth over time and/or the incorporation of mechanically eroded material from the upper plate. Beneath this part of the forearc, there is no bathymetric evidence for recent subduction related erosion, therefore this feature is consistent with the underplating suggested by *Fisher et al.* [1998] and *Morris et al.* [2002] as a mechanism to explain the low [10]Be concentrations in Costa Rican lavas. *Arroyo et al.*, [2009, 2014] came to a similar conclusion based on a large low-velocity anomaly they found in roughly the same location.

Due to the uncertainties associated in modeling the depth to the Cocos plate in this reflective area, we cannot be sure of exact nature of the reflective region. Velocities in the lower margin wedge are up to 6.7 km/s, which is much higher than the expected velocity of underplated material and explains the origins of reflections that occur at the top of this region. At 15 km depth, fluids from sediments and tectonically eroded materials are likely to be highly compacted and fluids expelled, so would the velocity contrast between the zone of underplating and the top of the Cocos plate produce a reflection? It is possible that continued fluid expulsion down dip from this region would result in fluid flow back up the plate boundary resulting in a reflective boundary. It is also possible that the reflections are a result of heterogeneities within the underplated materials such as the duplex structures observed by *Collot et al.* [2008] at ∼15 km depth offshore Ecuador.

Underplating beneath the inner-forearc beneath Costa Rica may be more widespread than imaged in our data. *Freundt et al.* [2014] estimated input and output fluxes of mineral bound H_2O along the entire Central American Volcanic Arc, and found that even if 20–30% of mineral bound water is subducted past magma generating depths, a 30–40% deficit still remains. Underplating of subducted materials may explain this deficit.

7. Conclusions

We have presented the results of a seismic reflection and refraction survey of the forearc offshore Costa Rica. The data are consistent with two similar models for the Cocos/Caribbean plate interface. One model shows a one-layer Cocos plate deepening to the SE with up to 4 km of relief over a 5 km distance; the depth

ranges from 15 km beneath Nicoya peninsula to 21 km further to the SE. The other model shows a two-layer Cocos plate with a slight SE dip at depths ranging from 15 to 18 km.

We also present an MCS reflection image showing margin-perpendicular normal faults cutting the BOSS horizon consistent with the inner-arc uplift observed by *Fisher et al.* [1998]. A zone of reflectivity in the MCS image at a depth that approximately coincides with the top of the Cocos plate suggests a region of under-plated material that is up to 3 km thick and 40 km wide. This material is likely a combination of sediments from the Cocos plate and tectonically eroded material from the outer forearc.

References

Albarède, F. (1998), The growth of continental crust, *Tectonophysics*, *296*, 1–14.

Alvarado, G. E., P. Denyer, and C. W. Sinton (1997), The 89 Ma Tortugal komatiitic suite, Costa Rica: Implications for a common geological origin of the Caribbean and Eastern Pacific region from a mantle plume, *Geology*, *25*, 439–442.

Arroyo, I. G., S. Husen, E. R. Flueh, J. Gossler, E. Kissling, and G. E. Alvarado (2009), Three-dimensional P-wave velocity structure on the shallow part of the Central Costa Rican Pacific margin from local earthquake tomography using off- and onshore networks, *Geophys. J. Int.*, *179*, 827–849.

Arroyo, I. G., S. Husen, and E. R. Flueh (2014), The seismogenic zone in the Central Costa Rican Pacific margin: High quality hypocentres from and amphibious network, *Int. J. Earth Sci.*, *103*, 1747–1764.

Barckhausen, U., C. R. Ranero, R. von Huene, S. C. Cande, and H. A. Roeser (2001), Revised tectonic boundaries in the Cocos Plate off Costa Rica: Implications for the segmentation of the convergent margin and for plate tectonic models, *J. Geophys. Res.*, *106*, 19,207–19,220, doi:10.1029/2001JB000238.

Buchs, D. M., R. J. Arculus, P. O. Baumgartner, C. Baumgartner-Mora, and A. Ulianov (2010), Late Cretaceous arc development on the SW margin of the Caribbean Plate: Insights from the Golfito, Costa Rica, and Azuero, Panama, complexes, *Geochem. Geophys. Geosyst.*, *11*, Q07S24, doi:10.1029/2009GC002901.

Carr, M. J., I. Saginor, G. E. Alvarado, L. L. Bolge, F. N. Lindsay, K. Milidakis, B. D. Turrin, M. D. Feigenson, and C. C. Swisher III (2007), Element fluxes from the volcanic front of Nicaragua and Costa Rica, *Geochem. Geophys. Geosyst.*, *8*, Q06001, doi:10.1029/2006GC001396.

Christeson, G. L., K. D. McIntosh, and T. H. Shipley (1999), Structure of the Costa Rica convergent margin, offshore Nicoya Peninsula, *J. Geophys. Res.*, *104*, 25,443–25,468, doi:10.1029/1999JB900251.

Clift, P. and J. H. Hartley (2007), Slow Rates of subduction erosion and coastal underplating along the Andean margin of Chile and Peru, *Geology*, *35*, 503–506.

Clift, P., and P. Vannucchi (2004), Controls on Tectonic accretion vs erosion in subduction zones: Implications for the origin and recycling of the continental crust, *Rev. Geophys.*, *42*, RG2001, doi:10.1029/2003RG000127.

Collot, J. Y., W. Agudelo, A. Ribodetti, and B. Marcaillou (2008), Origin of a crustal splay fault and its relation to the seismogenic zone and underplating at the erosional north Ecuador–south Colombia oceanic margin, *J. Geophys. Res.*, *113*, B12102, doi:10.1029/2008JB005691.

DeMets, C. (2001), A new estimate for present-day Cocos-Caribbean plate motion: Implications for slip along the Central American volcanic arc, *Geophys. Res. Lett.*, *28*, 4043–4046, doi:10.1029/2001GL013518.

Denyer, P., and E. Gazel (2009), The Costa Rican Jurassic to Miocene oceanic complexes: Origin, tectonics and relations, *J. South Am. Earth Sci.*, *28*, 429–442, doi:10.1016/j.jsames.2009.04.010.

Fisher, D. M., T. W. Gardner, J. S. Marshall, P. B Sak, and M. Protti (1998), Effect of subducting sea-floor roughness on fore-arc kinematics, Pacific coast, Costa Rica, *Geology*, *26*, 467–470.

Fisher, D. M., T. W. Gardner, P. B. Sak, J. D. Sanchez, K. Murphy, and P. Vannucchi (2004), Active thrusting in the inner forearc of an erosive convergent margin, Pacific coast, Costa Rica, *Tectonics*, *23*, TC2007 doi:10.1029/2002TC001464.

Freundt, A., I. Grevemeyer, W. Rabbel, T. H. Hansteen, C. Hensen, H. Whermann, S. Kutterolf, R. Halama, and M. Frische (2014), Volatile (H_2O, CO_2, Cl, S) budget of the Central American subduction zone, *Int. J. Earth Sci.*, *103*, 2101–2127.

Guinta, G., and L. Beccaluva (2006), Caribbean Plate margin evolution: Constraints and current problems, *Geol. Acta*, *4*, 265–277.

Hinz, K., R. von Huene, and C. R. Ranero (1996), Tectonic structure of the convergent Pacific margin offshore Costa Rica from multichannel seismic reflection data, *Tectonics*, *15*, 54–66, doi:10.1029/95TC02355.

Ivandic, M., I. Grevemeyer, J. Bialas, and C. J. Petersen (2010), Serpentinization in the trench-outer rise region offshore of Nicaragua: Constraints from seismic refraction and wide-angle data, *Geophys. J. Int.*, *180*, 1253–1264, doi:10.1111/j.1365-246X.2009.04474.x.

LaFemina, P., T. H. Dixon, R. Govers, E. Norabuena, H. Turner, A. Saballos, G. Mattioli, M. Protti, and W. Strauch (2009), Fore-arc motion and Cocos Ridge collision in Central America, *Geochem. Geophys. Geosyst.*, *10*, Q05S14, doi:10.1029/2008GC002181.

Meschede, M., P. Zweigel, and E. Kiefer (1999), Subsidence and extension at a convergent plate margin: Evidence for subduction erosion off Costa Rica, *Terra Nova*, *11*, 112–117.

Morris, J., R. Valentine, and T. Harrison (2002), [10]Be imaging of sediment accretion and subduction along the northeast Japan and Costa Rica convergent margins, *Geology*, *30*, 659–672.

Morris, J. D., W. P. Leeman, and F. Tera (1990), The subducted component in island arc lavas: Constraints from Be isotopes and B–Be systematics, *Nature*, *344*, 31–36.

Patino, L. C., M. J. Carr, and M. D. Feigenson (2000), Local and regional variations in central American arc lavas controlled by variations in subducted sediment input, *Contrib. Mineral. Petrol.*, *138*, 265–283.

Ramananantoandro, R., and N. Bernitsas (1987), A computer algorithm for automatic picking of refraction first-arrival time, *Geoexploration*, *24*, 147–151.

Ranero, C. R., and R. von Huene (2000), Subduction erosion along the Middle America convergent margin, *Nature*, *404*, 748–752.

Sak, P. B., D. M. Fisher, T. W. Gardner, J. S. Marshall, and P. C. LaFemina (2009), Rough crust subduction, forearc kinematics, and Quaternary uplift rates, Costa Rican segment of the Middle American Trench, *Geol. Soc. Am. Bull.*, *121*, 992–1012.

Schmidt, M. W., and S. Poli (1998), Experimentally based water budgets for dehydrating slabs and consequences for arc magma generation, *Earth Planet. Sci. Lett.*, *163*, 361–379.

Scholl, D. W., and R. von Huene (2007), Crustal recycling at modern subduction zones applied to the past: Issues of growth and preservation of continental basement crust, mantle geochemistry, and supercontinent reconstruction, in *4-D Framework of Continental Crust ISBN: 978-0-8137-1200-0*, edited by R. D. Hatcher. Jr. et al., *Mem. Geol. Soc. Am.*, *200*, 9–32.

Shreve, R. L., and M. Cloos (1986), Dynamics of sediment subduction, melange formatino, and prism accretion, *J. Geophys. Res.*, *91*, 10,229–10,245.

Sinton, C. W., A. D. Duncan, and P. Denyer (1997), Nicoya Peninsula, Costa Rica: A single suite of Caribbean oceanic plateau magmas, *J. Geophys. Res.*, *102*, 15,507–15,520, doi:10.1029/97JB00681.

Vannucchi, P., D. W. Scholl, M. Meschede, and K. McDougall-Ried (2001), Tectonic erosion and consequent collapse of the Pacific margin of Costa Rica: Combined implications from ODP Leg 170, seismic offshore data, and regional geology of the Nicoya Peninsula, *Tectonics*, *20*, 649–668, doi:10.1029/2000TC001223.

Vannucchi, P., C. R. Ranero, S. Galeotti, S. M. Straub, D. W. Scholl, and K. McDougall-Ried (2003), Fast rates of subduction erosion along the Costa Rica Pacific margin: Implications for nonsteady rates of crustal recycling at subduction zones, *J. Geophys. Res.*, *108*(B11), 2511, doi:10.1029/2002JB002207.

Vannucchi, P., F. Sage, J. P. Morgan, F. Remitti, and J. Collot (2012), Toward a dynamic concept of the subduction channel at erosive convergent margins with implications for interplate material transfer, *Geochem. Geophys. Geosyst.*, *13*, Q02003, doi:10.1029/2011GC003864.

Van Avendonk, H. J. A., A. J. Harding, J. A. Orcutt, and J. S. McClain (1998), A two-dimensional tomographic study of the Clipperton transform fault, *J. Geophys. Res.*, *103*, 17,885–17,899, doi:10.1029/98JB00904.

Van Avendonk, H. J. A., D. J. Shillington, W. S. Holbrook, and M. J. Hornbach (2004), Inferring crustal structure in the Aleutian arc from a sparse wide-angle seismic data set, *Geochem. Geophys. Geosyst.*, *5*, Q08008, doi:10.1029/2003GC000664.

Van Avendonk, H. J. A., W. S. Holbrook, D. Lizarralde, and P. Denyer (2011), Structure and serpentinization of the subducting Cocos plate offshore Nicaragua and Costa Rica, *Geochem. Geophys. Geosyst.*, *12*, Q06009, doi:10.1029/2011GC003592.

von Huene, R., and D. W. Scholl (1991), Observations at convergent margins concerning sediment subduction, subduction erosion, and the growth of continental crust, *Rev. Geophys.*, *29*, 279–316, doi:10.1029/91RG00969.

von Huene, R., C. R. Ranero, W. Weinrebe, and K. Hinz (2000), Quaternary convergent margin tectonics of Costa Rica, segmentation of the Cocos Plate, and Central American volcanism, *Tectonics*, *19*, 314–334, doi:10.1029/1999TC001143.

von Huene, R., C. R. Ranero, and P. Vannucchi (2004), Generic model of subduction erosion, *Geology*, *32*, 913–916, doi:10.1130/G20563.1.

Walther, C. H. E. (2003), The crustal structure of the Cocos ridge off Costa Rica, *J. Geophys. Res.*, *108*(B3), 2136, doi:10.1029/2001JB000888.

Werner, R., K. Hoernle, P. van den Bogaard, C. R. Ranero, R. von Huene, and D. Korich (1999), Drowned 14 m.y. old Galapagos archipelago off the coast of Costa Rica: Implications for tectonic and evolutionary models, *Geology*, *27*, 499–502.

Werner, R., K. Hoernle, U. Barckhausen, and F. Hauff (2003), Geodynamic evolution of the Galápagos hot spot system (Central East Pacific) over the past 20 m.y.: Constraints from morphology, geochemistry, and magnetic anomalies, *Geochem. Geophys. Geosyst.*, *4*(12), 1108, doi:10.1029/2003GC000576.

Ye, S., J. Bialas, E.R. Flueh, A. Stavenhagen, R. von Huene, G. Leandro, and K. Hinz (1996), Crustal structure of the Middle American Trench off Costa Rica from wide-angle seismic data, *Tectonics*, *15*, 1006–1021, doi:10.1029/96TC00827.

Zelt, C. A. and R. B. Smith (1992), Seismic travel-time inversion for 2-D crustal velocity structure, *Geophys. J. Int.*, *108*, 16–34.

Zhu, J., H. Kopp, E.R. Flueh, D. Klaeschen, C. Papenberg, and L. Planert (2009), Crustal structure of the central Costa Rica subduction zone: Implications for basal erosion from seismic wide-angle data, *Geophys. J. Int.*, *178*, 1112–1131.